SEMARAK ILMU PUBLISHING

CFD Letters

Journal homepage:
https://semarakilmu.com.my/journals/index.php/CFD_Letters/index
ISSN: 2180-1363

The Influence of Limiters on Davis-Yee and Harten-Yee TVD Schemes

Siti Aisyah Alimuddin[1], Iman Fitri Ismail[1], Akmal Nizam Mohammed[2,*], Bambang Basuno[1]

[1] Aerodynamics and Propulsion Research Group, Universiti Tun Hussein Onn Malaysia, 86400 Parit Raja, Batu Pahat, Johor, Malaysia
[2] Combustion Research Group, Universiti Tun Hussein Onn Malaysia, 86400 Parit Raja, Batu Pahat, Johor, Malaysia

ARTICLE INFO

Article history:
Received 25 April 2022
Received in revised form 20 July 2022
Accepted 11 August 2022
Available online 30 September 2022

Keywords:
Euler solver; TVD scheme; shock wave

ABSTRACT

TVD schemes have many selections of limiters, but the recommendation of limiters for specific cases is not available in the literature. This study focuses on incorporating two flux limiters as the extension of the TVD schemes proposed by Harten-Yee and Davis-Yee and extends the test case on external flows, blunt-body. The method used in this study is Harten-Yee Upwind TVD and Davis-Yee Symmetric TVD scheme with different limiter functions to simulate cases for two-dimensional compressible flow. The results show that all the limiter functions can capture shock waves when the flow passes through the geometry at Mach number $Ma = 2.0$. The flow features such as bow shock, oblique shock, shock wave reflection, interaction, and expansion wave can all be captured in the case of the bump in a channel and wedge. While in the case of the external supersonic flow passing through the blunt-body, the presence of a bow shock was captured. We discovered that Davis-Yee limiter number 2 performs significantly better than other proposed Davis-Yee and Harten-Yee limiters for the case in this study. Therefore, the Davis-Yee Upwind TVD method is recommended to be applied for the identical case on the expansion of this study.

1. Introduction

Considering recent advances in aerospace engineering, current research focuses on supersonic and hypersonic flow domains. These engineering applications surpassed the Mach number of 0.3, where compressibility effects are no longer negligible [1]. As the Mach number increases, the variation in density within the flow becomes even more prominent [2]. The transition from an incompressible to a compressible state resulted in fascinating physical phenomena, which include shockwaves and contact discontinuities. In addition, the greater the Reynolds number of a flow, the thinner its boundary layers are relative to its streamlined size, which gives the flow an inviscid assumption due to the small dimension of its viscous region [3].

A significant amount of research and development has been done to perfect methods for capturing the sharp gradients associated with shock waves and contact discontinuities in compressible fluid flow. Total variation diminishing (TVD), essentially non-oscillatory (ENO), and weighted essentially non-oscillatory (WENO) are the most often used shock-capturing schemes.

* *Corresponding author.*
E-mail address: akmaln@uthm.edu.my (Akmal Nizam Mohammed)

https://doi.org/10.37934/cfdl.14.9.1531

Due to high performance and parallel scalability, explicit Runge-Kutta schemes are the most often utilized time discretization for hyperbolic partial differential equations (PDEs) [4]. The explicit Runge-Kutta scheme prevents the inversion of large nonlinear systems by spatial discretizations [5]. Fourth-order Runge-Kutta scheme with central differencing of the convective term has a stability requirement $c \leq 2\sqrt{2}$, exceeding the stability requirement, $c \leq 1$ of most linear hyperbolic equations. Damping term needs to be included for nonlinear hyperbolic equations to stabilize the solution as the scheme may be unstable when central differencing of the convective term is used [6]. Another scheme that can reduce the dispersion error that appears as oscillation other than an artificial viscosity term in the equation is the TVD scheme.

Total variation Diminishing (TVD) scheme possesses properties needed to compute domains with discontinuities. The fundamental advantage of TVD schemes is that no additional artificial viscosity is required, and they can suppress the spurious numerical oscillation across discontinuities [7]. TVD schemes eliminate the oscillations within the domain while reducing the shock-smearing. However, the numerical solutions may not be free of oscillations as a high-order scheme could cause oscillations and overshoots under highly convective conditions [8,9]. Yee [10] presented a new implicit, unconditionally stable, high-resolution TVD scheme for steady-state calculations that are not generating spurious oscillations for a constant coefficient system and a nonlinear scalar equation. The accuracy and monotonicity are preserved by the Second-Order TVD schemes using limiter functions [11]. In a particular advection case, different limiters may operate differently.

The modified Fourth-Order Runge-Kutta scheme uses a central difference approximation that may generate a significant dispersion error in the vicinity of sharp flow gradients, referred to as shock waves. Therefore, a post-processor that provides a way to add artificial dissipation mechanisms must be added to reduce oscillations in the solution [12]. TVD-limiters are selected as the artificial dissipation mechanisms in the present research.

Harten-Yee Upwind TVD and Davis-Yee Symmetric TVD are two out of various second-order TVD schemes. In order to evaluate high-resolution numerical solutions in smooth regions and sharp results in the vicinity of shocks and discontinuities, high-resolution schemes are developed [13]. Harten constructs high-resolution TVD schemes by applying modified flux to a first-order TVD scheme [14]. The scheme is second-order in smoothness regions and first-order in extrema points due to the modified flux.

At each iteration level, the solution is enhanced with a Total Variation Diminishing (TVD) model in a post-process stage to stabilize it after modified Fourth-Order Runge-Kutta was applied to solve problems [15]. The modified Runge-Kutta scheme is then presented, followed by a description of the Davis-Yee symmetric TVD model in the methodology.

The Fourth-Order Runge-Kutta scheme consists of four steps, and the last step is the TVD scheme's implementation. Various TVD schemes have been developed, such as Harten-Yee Upwind TVD, Roe-Sweby Upwind TVD, Davis-Yee Symmetric TVD, and MacCormack TVD schemes. Harten-Yee Upwind TVD and Davis-Yee Symmetric TVD schemes will be utilized in this study. Hence the Modified Fourth-Order Runge Kutta augmented with TVD is applied to the flow passing through wedge, blunt-body, and bump in a channel. Wedge and bump in a channel belong to the internal flow problem, while blunt-body belongs to the external flow problem. This study will discuss the fluid flow with Mach number $Ma = 2.0$.

Harten-Yee and Davis-Yee have made significant contributions to the development of two of the most well-known techniques for TVD. On a numerical level, it is commonly acknowledged that these particular techniques have been replaced by newer, more stable, and computationally inexpensive solvers. Therefore, the purpose of this study is not to design a solver that surpasses the capabilities of existing CFD codes, but to investigate the possibilities of enhancing the shock-capture method by

comparing the flux limiters. Due to the inherent nature of high-order linear schemes, which create spurious oscillations in the region of discontinuities and shocks inside the solution, nonlinear approaches, such as flux or slope limiters, are implemented to mitigate these shortcomings. The prior study was limited to a single flux limiter, as illustrated by Eq. (32) and Eq. (33), and only internal flow within the wedge was considered [16].

As an extension of the TVD schemes proposed by Harten-Yee and Davis-Yee, this study aims to incorporate two flux limiters and extend the test of external flows on different geometries. To emulate the scheme's ability to record compression and expansion waves in an internal flow, the numerical analysis of these TVD schemes is extended to include a bump in a channel. Furthermore, in order to model bow shocks, the blunt-body geometry, which involves an external flow, is also examined. Finally, the performance of these several limiters is evaluated and compared to identify the flux limiter with the highest efficiency.

2. Governing Equation of Fluid Motion

The governing equation of motion for two-dimensional inviscid compressible flow in vector notation is written as:

$$\frac{\partial Q}{\partial t}+\frac{\partial E}{\partial x}+\frac{\partial F}{\partial y}=0 \tag{1}$$

Where

$$Q=\begin{bmatrix}\rho\\ \rho u\\ \rho v\\ \rho e_t\end{bmatrix}, E=\begin{bmatrix}\rho u\\ \rho u^2+p\\ \rho uv\\ (\rho e_t+\rho)u\end{bmatrix}, F=\begin{bmatrix}\rho v\\ \rho vu\\ \rho v^2+p\\ (\rho e_t+\rho)v\end{bmatrix} \tag{2}$$

In the equation above, the definition of variables can be described as follows. The variable Q is the vector of conserved variables, while E and F represent the flux vectors. The air density is ρ, the component of velocity in x and y axis-direction are denoted respectively as u and v. The static pressure p and the total energy e_t. Eq. (2) represents a system equation that contains four nonlinear differential equations with five unknowns (ρ, u, v, p , e_t). Hence, other relationships are required to become five equations with five unknowns. The additional relation can be used from the relationship between the total internal energy e_t with other flow variables defined as:

$$e_t=e+\frac{u^2+v^2}{2} \tag{3}$$

The flow problems can be solved by directly solving Eq. (2). However, due to a complex flow domain and eliminating the difficulties in implementing the boundary conditions, one may require transforming Eq. (2) in the form of the equation in curvilinear coordinates [17]. The Euler equation in a curvilinear coordinate can be referred to in a paper by Hixon *et al.,* [18].

3. Methodology

The previous subchapter stated various numerical schemes were developed to solve the Euler equation. This study adopts the method introduced by Hoffmann called the Modified Fourth-Order Runge Kutta augmented with TVD. Although the flow problem is a steady flow problem, the governing equation used is the governing equation in unsteady form by the existence of the time derivative term. This approach is applied to make the governing equation over the whole flow domain behave as an utterly hyperbolic differential equation, and a time marching approach to the steady-state solution can be adopted. In this time marching approach, the calculation is from time step $t = t^n$ to $t = t^{n+1}$, starts with the Fourth-Order Runge-Kutta scheme, followed by the TVD scheme to update the flow variables obtained by the Runge-Kutta before continuing to the next following time step. These two methods will be described in the following subchapter.

3.1 The Fourth-Order Runge-Kutta Scheme

If the conserved variable $Q_{i,j}^n$at any control point i, j at any time level known $t = t^n$, then to update that conserved variables as the quantities at the time level $t = t^{n+1}$. Hence, the Euler equation, Eq. (2), in view of the Fourth-Order Runge-Kutta scheme, becomes

$$\bar{Q}_{i,j}^{(1)} = \bar{Q}_{i,j}^n \tag{4}$$

$$\bar{Q}_{i,j}^{(2)} = \bar{Q}_{i,j}^n - \frac{\Delta\tau}{4}\left[\left(\frac{\partial\bar{E}}{\partial\xi}\right)_{i,j}^{(1)} + \left(\frac{\partial\bar{F}}{\partial\eta}\right)_{i,j}^{(1)}\right] \tag{5}$$

$$\bar{Q}_{i,j}^{(3)} = \bar{Q}_{i,j}^n - \frac{\Delta\tau}{3}\left[\left(\frac{\partial\bar{E}}{\partial\xi}\right)_{i,j}^{(2)} + \left(\frac{\partial\bar{F}}{\partial\eta}\right)_{i,j}^{(2)}\right] \tag{6}$$

$$\bar{Q}_{i,j}^{(4)} = \bar{Q}_{i,j}^n - \frac{\Delta\tau}{2}\left[\left(\frac{\partial\bar{E}}{\partial\xi}\right)_{i,j}^{(3)} + \left(\frac{\partial\bar{F}}{\partial\eta}\right)_{i,j}^{(3)}\right] \tag{7}$$

$$\bar{Q}_{i,j}^{(n+1)} = \bar{Q}_{i,j}^n - \Delta\tau\left[\left(\frac{\partial\bar{E}}{\partial\xi}\right)_{i,j}^{(4)} + \left(\frac{\partial\bar{F}}{\partial\eta}\right)_{i,j}^{(4)}\right] \tag{8}$$

The variable $\bar{Q}$ is the vector of conserved variables, while $\bar{E}, \bar{F}$ represent the flux vectors. Viscous stress is τ.In the next following steps, the obtained values $\bar{Q}_{i,j}^{(n+1)}$ will be used as the value conserved variables in the TVD scheme.

3.2 Second-Order TVD Formulation

The second-order TVD scheme for the quasi-one-dimensional Euler equation is extended to the two-dimensional Euler equation, and the finite-difference equation is written as follows [8].

$$\bar{Q}_{i,j}^{n+1} = \bar{Q}_i^n - \frac{\Delta\tau}{\Delta\xi}\left[\left(R_\xi\right)_{i+\frac{1}{2}j}^n - \left(R_\xi\right)_{i-\frac{1}{2}j}^n\right] - \frac{\Delta\tau}{\Delta\eta}\left[\left(R_\eta\right)_{i,j+\frac{1}{2}}^n - \left(R_\eta\right)_{i,j-\frac{1}{2}}^n\right] \tag{9}$$

Where

$$\left(R_{\xi}\right)_{i+\frac{1}{2}j}^{n}=\frac{1}{2}\left[\bar{E}_{i+1j}^{n}+\bar{E}_{i,j}^{n}+\left(X_{A}\right)_{i+\frac{1}{2}j}^{n}\left(\phi_{\xi}\right)_{i+\frac{1}{2}j}^{n}\right] \tag{10}$$

$$\left(R_{\xi}\right)_{i-\frac{1}{2}j}^{n}=\frac{1}{2}\left[\bar{E}_{i,j}^{n}+\bar{E}_{i-1j}^{n}+\left(X_{A}\right)_{i-\frac{1}{2}j}^{n}\left(\phi_{\xi}\right)_{i-\frac{1}{2}j}^{n}\right] \tag{11}$$

$$\left(R_{\xi}\right)_{i,j+\frac{1}{2}}^{n}=\frac{1}{2}\left[\bar{F}_{i,j+1}^{n}+\bar{F}_{i,j}^{n}+\left(X_{B}\right)_{i,j+\frac{1}{2}}^{n}\left(\phi_{\xi}\right)_{i+,j+\frac{1}{2}}^{n}\right] \tag{12}$$

$$\left(R_{\xi}\right)_{i,j-\frac{1}{2}}^{n}=\frac{1}{2}\left[\bar{F}_{i,j}^{n}+\bar{F}_{i,j-1}^{n}+\left(X_{B}\right)_{i,j-\frac{1}{2}}^{n}\left(\phi_{\xi}\right)_{i+,j-\frac{1}{2}}^{n}\right] \tag{13}$$

In the second term, on the right-hand side of Eq. (9) and all quantities appear in Eq. (10) to Eq. (13) are calculated according to the quantity $\bar{Q}_{i,j}^{(n+1)}$. In view of the TVD scheme, the difference between one variant of the TVD scheme with another variant TVD scheme is in terms of the flux limiter vectors $\left[\left(\Phi_{\xi}\right)_{i+\frac{1}{2}j}^{n},\left(\Phi_{\xi}\right)_{i+\frac{1}{2}j}^{n}\right]$ and $\left[\left(\Phi_{\eta}\right)_{i,j+\frac{1}{2}}^{n},\left(\Phi_{\eta}\right)_{i,j-\frac{1}{2}}^{n}\right]$. In this respect, one may recognize the presence of the Harten-Yee TVD scheme, Davis-Yee TVD scheme, and Roe-Sweby TVD scheme. As mentioned in the previous subchapter, the present work uses a first and second-order TVD scheme.

3.2.1 Harten-Yee upwind TVD

The general expressions for the component of the flux limiter vectors are defined as

$$\left(\Phi_{\xi}\right)_{i+\frac{1}{2}j}^{n}=\sigma\left[\left(\alpha_{\xi}\right)_{i+\frac{1}{2}j}\right]\left[\left(G_{\xi}\right)_{i+1j}+\left(G_{\xi}\right)_{i,j}\right]-\psi\left[\left(\alpha_{\xi}\right)_{i+\frac{1}{2}j}+\left(\beta_{\xi}\right)_{i+\frac{1}{2}j}\right]\left(\delta_{\xi}\right)_{i+\frac{1}{2}j} \tag{14}$$

$$\left(\Phi_{\xi}\right)_{i-\frac{1}{2}j}^{n}=\sigma\left[\left(\alpha_{\xi}\right)_{i-\frac{1}{2}j}\right]\left[\left(G_{\xi}\right)_{i,j}+\left(G_{\xi}\right)_{i-1j}\right]-\psi\left[\left(\alpha_{\xi}\right)_{i-\frac{1}{2}j}+\left(\beta_{\xi}\right)_{i-\frac{1}{2}j}\right]\left(\delta_{\xi}\right)_{i-\frac{1}{2}j} \tag{15}$$

$$\left(\Phi_{\eta}\right)_{i,j+\frac{1}{2}}^{n}=\sigma\left[\left(\alpha_{\eta}\right)_{i,j+\frac{1}{2}}\right]\left[\left(G_{\eta}\right)_{i,j+1}+\left(G_{\eta}\right)_{i,j}\right]-\psi\left[\left(\alpha_{\eta}\right)_{i,j+\frac{1}{2}}+\left(\beta_{\eta}\right)_{i,j+\frac{1}{2}}\right]\left(\delta_{\eta}\right)_{i,j+\frac{1}{2}} \tag{16}$$

$$\left(\Phi_{\eta}\right)_{i,j-\frac{1}{2}}^{n}=\sigma\left[\left(\alpha_{\eta}\right)_{i,j-\frac{1}{2}}\right]\left[\left(G_{\eta}\right)_{i,j-1}+\left(G_{\eta}\right)_{i,j}\right]-\psi\left[\left(\alpha_{\eta}\right)_{i,j-\frac{1}{2}}+\left(\beta_{\eta}\right)_{i,j-\frac{1}{2}}\right]\left(\delta_{\eta}\right)_{i,j-\frac{1}{2}} \tag{17}$$

In the context of limiter function, G, five limiters will be used for Harten-Yee. The limiters are in the form of x-direction and y-direction as follows.

The first limiter

$$\left(G_{\xi}\right)_{i,j}=minmod\left[\left[\left(\delta_{\xi}\right)_{i-\frac{1}{2}j},\left(\delta_{\xi}\right)_{i+\frac{1}{2}j}\right]\right] \tag{18}$$

$$\left(G_{\eta}\right)_{i,j}=minmod\left[\left[\left(\delta_{\eta}\right)_{i,j-\frac{1}{2}},\left(\delta_{\eta}\right)_{i,j+\frac{1}{2}}\right]\right] \tag{19}$$

Second limiter

$$(G_\xi)_{i,j} = \frac{(\delta\xi)_{i+\frac{1}{2}j}(\delta\xi)_{i-\frac{1}{2}j}+\left[(\delta\xi)_{i+\frac{1}{2}j}(\delta\xi)_{i-\frac{1}{2}j}\right]}{(\delta\xi)_{i+\frac{1}{2}j}+(\delta\xi)_{i-\frac{1}{2}j}} \tag{20}$$

$$(G_\eta)_{i,j} = \frac{(\delta\eta)_{i,j+\frac{1}{2}}(\delta\eta)_{i,j-\frac{1}{2}}+\left[(\delta\eta)_{i,j+\frac{1}{2}}(\delta\eta)_{i,j-\frac{1}{2}}\right]}{(\delta\eta)_{i,j+\frac{1}{2}}+(\delta\eta)_{i,j-\frac{1}{2}}} \tag{21}$$

Third limiter

$$(G_\xi)_{i,j} = \frac{(\delta\xi)_{i-\frac{1}{2}j}\left\{\left[(\delta\xi)_{i+\frac{1}{2}j}\right]^2+\omega\right\}+(\delta\xi)_{i+\frac{1}{2}j}\left\{\left[(\delta\xi)_{i-\frac{1}{2}j}\right]^2+\omega\right\}}{\left[(\delta\xi)_{i+\frac{1}{2}j}\right]^2+\left[(\delta\xi)_{i-\frac{1}{2}j}\right]^2+2\omega} \tag{22}$$

$$(G_\eta)_{i,j} = \frac{(\delta\eta)_{i,j-\frac{1}{2}}\left\{\left[(\delta\eta)_{i,j+\frac{1}{2}}\right]^2+\omega\right\}+(\delta\eta)_{i,j+\frac{1}{2}}\left\{\left[(\delta\eta)_{i,j-\frac{1}{2}}\right]^2+\omega\right\}}{\left[(\delta\eta)_{i,j+\frac{1}{2}}\right]^2+\left[(\delta\eta)_{i,j-\frac{1}{2}}\right]^2+2\omega} \tag{23}$$

Fourth limiter

$$(G_\xi)_{i,j} = minmod\left\{2(\delta\xi)_{i-\frac{1}{2}j}, 2(\delta\xi)_{i+\frac{1}{2}j}, \frac{1}{2}\left[(\delta\xi)_{i+\frac{1}{2}j}+(\delta\xi)_{i-\frac{1}{2}j}\right]\right\} \tag{24}$$

$$(G_\eta)_{i,j} = minmod\left\{2(\delta\eta)_{i,j-\frac{1}{2}}, 2(\delta\eta)_{i,j+\frac{1}{2}}, \frac{1}{2}\left[(\delta\eta)_{i,j+\frac{1}{2}}+(\delta\eta)_{i,j-\frac{1}{2}}\right]\right\} \tag{25}$$

And the fifth limiter

$$(G_\xi)_{i,j} = Sgn * max\left\{0, min\left[2\left|(\delta\xi)_{i+\frac{1}{2}j}\right|, Sgn*(\delta\xi)_{i-\frac{1}{2}j}\right], min\left[\left|(\delta\xi)_{i+\frac{1}{2}j}\right|, 2Sgn*(\delta\xi)_{i-\frac{1}{2}j}\right]\right\} \tag{26}$$

$$(G_\eta)_{i,j} = Sgn * max\left\{0, min\left[2\left|(\delta\eta)_{i,j+\frac{1}{2}}\right|, Sgn*(\delta\eta)_{i,j-\frac{1}{2}}\right], min\left[\left|(\delta\eta)_{i,j+\frac{1}{2}}\right|, 2Sgn*(\delta\eta)_{i,j-\frac{1}{2}}\right]\right\} \tag{27}$$

3.2.2 Davis-Yee symmetric TVD

The general expressions for the component of the flux limiter vectors are

$$\left(\Phi_\xi\right)^n_{i+\frac{1}{2}j} = -\left\{\frac{\Delta t}{\Delta\xi}\left[\left(\alpha_\xi\right)_{i+\frac{1}{2}j}\right]^2\left(G_\xi\right)_{i+\frac{1}{2}j}+\psi\left[\left(\alpha_\xi\right)_{i+\frac{1}{2}j}\right]\left[\left(\delta_\xi\right)_{i+\frac{1}{2}j}-\left(G_\xi\right)_{i+\frac{1}{2}j}\right]\right\} \tag{28}$$

$$\left(\Phi_\xi\right)^n_{i-\frac{1}{2}j} = -\left\{\frac{\Delta t}{\Delta\xi}\left[\left(\alpha_\xi\right)_{i-\frac{1}{2}j}\right]^2\left(G_\xi\right)_{i-\frac{1}{2}j}+\psi\left[\left(\alpha_\xi\right)_{i-\frac{1}{2}j}\right]\left[\left(\delta_\xi\right)_{i-\frac{1}{2}j}-\left(G_\xi\right)_{i-\frac{1}{2}j}\right]\right\} \tag{29}$$

$$\left(\Phi_{\eta}\right)_{i,j+\frac{1}{2}}^{n} = -\left\{\frac{\Delta t}{\Delta \eta}\left[\left(\alpha_{\eta}\right)_{i,j+\frac{1}{2}}\right]^{2}\left(G_{\eta}\right)_{i,j+\frac{1}{2}} + \psi\left[\left(\alpha_{\eta}\right)_{i,j+\frac{1}{2}}\right]\left[\left(\delta_{\eta}\right)_{i,j+\frac{1}{2}} - \left(G_{\eta}\right)_{i,j+\frac{1}{2}}\right]\right\} \tag{30}$$

$$\left(\Phi_{\eta}\right)_{i,j-\frac{1}{2}}^{n} = -\left\{\frac{\Delta t}{\Delta \eta}\left[\left(\alpha_{\eta}\right)_{i,j-\frac{1}{2}}\right]^{2}\left(G_{\eta}\right)_{i,j-\frac{1}{2}} + \psi\left[\left(\alpha_{\eta}\right)_{i,j-\frac{1}{2}}\right]\left[\left(\delta_{\eta}\right)_{i,j-\frac{1}{2}} - \left(G_{\eta}\right)_{i,j-\frac{1}{2}}\right]\right\} \tag{31}$$

Similar to the Harten-Yee TVD scheme, this scheme also has a different model of limiter function. There are three limiters used for the Davis-Yee TVD scheme. These three limiter functions are defined as:

The first limiter

$$\left(G_{\xi}\right)_{i+\frac{1}{2}j} = minmod\left\{2\left(\delta_{\xi}\right)_{i-\frac{1}{2}j}, 2\left(\delta_{\xi}\right)_{i+\frac{1}{2}j}, 2\left(\delta_{\xi}\right)_{i+\frac{3}{2}j}, \frac{1}{2}\left[\left(\delta_{\xi}\right)_{i-\frac{1}{2}j}, \left(\delta_{\xi}\right)_{i+\frac{3}{2}j}\right]\right\} \tag{32}$$

$$\left(G_{\eta}\right)_{i,j+\frac{1}{2}} = minmod\left\{2\left(\delta_{\eta}\right)_{ij-\frac{1}{2}}, 2\left(\delta_{\eta}\right)_{i,j+\frac{1}{2}}, 2\left(\delta_{\eta}\right)_{i,j+\frac{3}{2}}, \frac{1}{2}\left[\left(\delta_{\eta}\right)_{i,j-\frac{1}{2}}, \left(\delta_{\eta}\right)_{i,j+\frac{3}{2}}\right]\right\} \tag{33}$$

Second limiter

$$\left(G_{\xi}\right)_{i+\frac{1}{2}j} = minmod\left\{\left(\delta_{\xi}\right)_{i-\frac{1}{2}j}, \left(\delta_{\xi}\right)_{i+\frac{1}{2}j}, \left(\delta_{\xi}\right)_{i+\frac{3}{2}j}\right\} \tag{34}$$

$$\left(G_{\eta}\right)_{i,j+\frac{1}{2}} = minmod\left\{\left(\delta_{\eta}\right)_{i,j-\frac{1}{2}}, \left(\delta_{\eta}\right)_{i,j+\frac{1}{2}}, \left(\delta_{\eta}\right)_{i,j+\frac{3}{2}}\right\} \tag{35}$$

Third limiter

$$\left(G_{\xi}\right)_{i+\frac{1}{2}j} = minmod\left[\left(\delta_{\xi}\right)_{i+\frac{1}{2}j}, \left(\delta_{\xi}\right)_{i-\frac{1}{2}j}\right] + minmod\left[\left(\delta_{\xi}\right)_{i+\frac{1}{2}j}, \left(\delta_{\xi}\right)_{i+\frac{3}{2}j}\right] - \left(\delta_{\xi}\right)_{i+\frac{1}{2}j} \tag{36}$$

$$\left(G_{\eta}\right)_{i,j+\frac{1}{2}} = minmod\left[\left(\delta_{\eta}\right)_{i,j+\frac{1}{2}}, \left(\delta_{\eta}\right)_{i,j-\frac{1}{2}}\right] + minmod\left[\left(\delta_{\eta}\right)_{i,j+\frac{1}{2}}, \left(\delta_{\eta}\right)_{i,j+\frac{3}{2}}\right] - \left(\delta_{\eta}\right)_{i,j+\frac{1}{2}} \tag{37}$$

3.2.3 Geometry

The first Euler solver, Fourth-Order Runge-Kutta with Harten-Yee Upwind TVD, allows one to choose one limiter function from five available limiter functions defined by Eq. (18) to Eq. (31). At the same time, the second Euler solver, Fourth-Order Runge-Kutta with Davis-Yee Symmetric TVD enables one to select one of the three available limiter functions, as stated in Eq. (32) to Eq. (37). These two Euler solvers are then applied to the case of two internal flow problems (bump in a channel and wedge) and one external flow problem (blunt-body). Finally, all the flow problems under consideration are set to have the flow condition at the flow Mach number, $M = 2.0$.

It is necessary to be noted that these two Euler solvers required a meshing over the flow domain. In the case of the internal flow along the bump in a channel, the required meshing flow domain is depicted in Figure 1. The geometry of the bump is adapted from a paper by Demirdžić *et al.,* [19]. In the case of internal flow along the wedge, the meshing flow domain is used, as shown in Figure 2. Figure 3 is blunt-body grid generation which involves external flow. The solid domain can be

mesh with a coarser size if the fluid domain is mesh with a finer size [20]. The previous computer codes used to solve the wedge flow problem have been modified by adding surface angles on the upper boundary. Table 1 shows the characteristics of the geometry used.

Table 1
Characteristics of geometry

	Bump in a channel	Wedge	Blunt-body
Mesh (x,y)	97×33	169×88	96×60
Flow problem	Internal	Internal	External

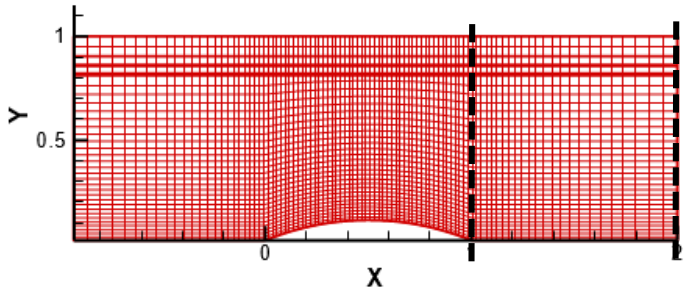

Fig. 1. Bump in a channel grid generation

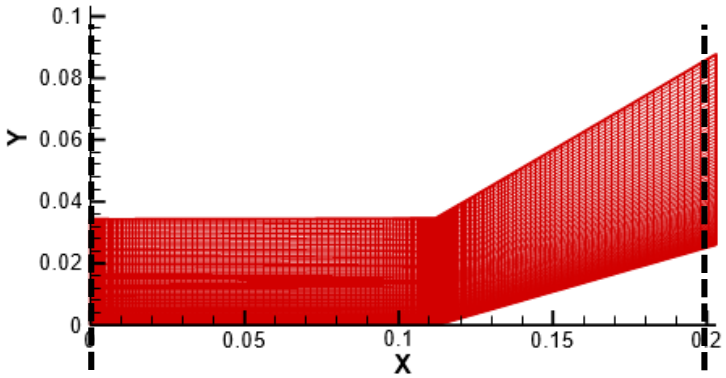

Fig. 2. Wedge grid generation

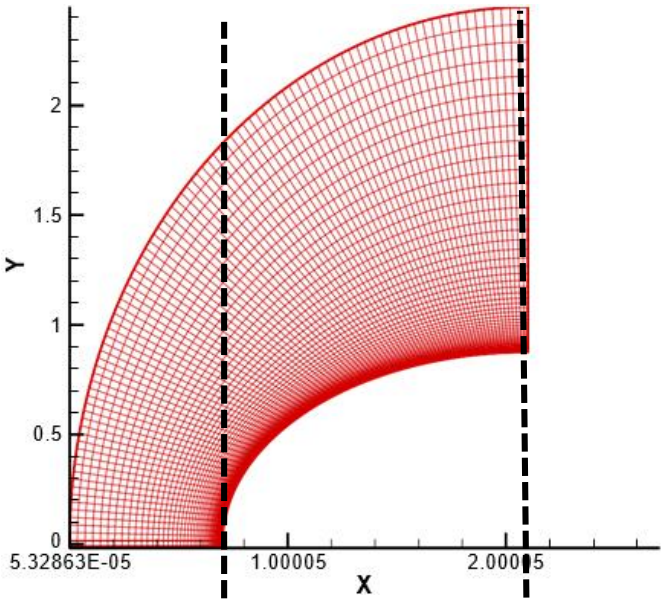

Fig. 3. Blunt-body grid generation

3.2.4 Grid independence test

A grid independence test was performed to discover the optimum grid size for this study. In addition, it shows us the limit to which we must refine our mesh to get accurate results since further refining the mesh would only increase computational time. Table 2 shows the grid sizes tested.

Table 2
Grid sizes to be tested

	Bump in a channel	Wedge	Blunt-body
Grid 1	87×33	169×88	96×60
Grid 2	77×33	149×88	86×60
Grid 3	97×33	129×88	76×60
Grid 4	97×43	169×68	96×50
Grid 5	97×53	169×108	96×70
Grid 6	-	169×128	96×80

The grid sizes were tested to determine the effect on the pressure distribution at a selected position (Figure 1, Figure 2 and Figure 3), as shown in Figure 4(a), Figure 5(a) and Figure 6(a). It was found that there are no significant changes in pressure distribution beyond the grid size of 97×33 (3201 as Grid 3) which is shown in Figure 4(a) and can be seen clearly in Figure 4(b). Figure 4(b) shows the highest pressure occurs at a specific point chosen as presented in terms of dimensionless form by dividing with the pressure obtained at grid size 2541. Therefore, for the numerical simulation, the grid size of 3201 has been used to perform simulation for the bump in a channel geometry.

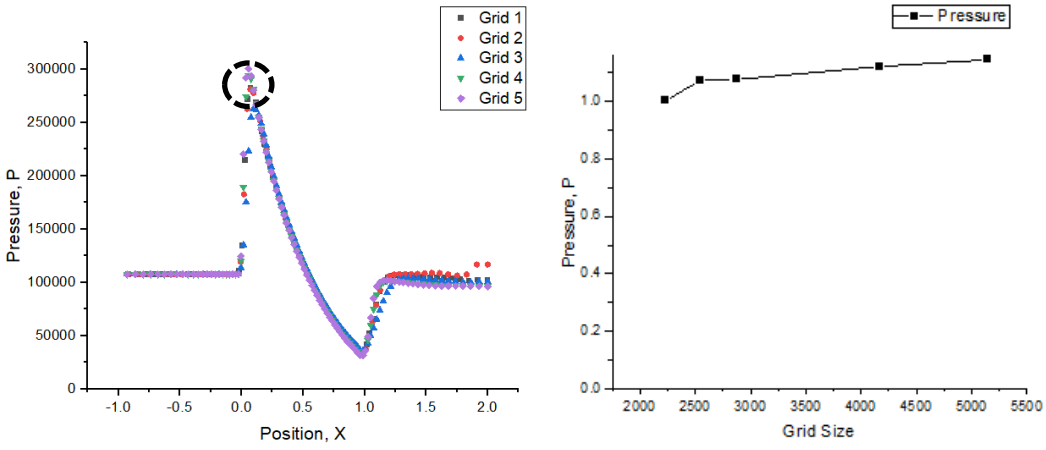

(a) (b)

Fig. 4. Comparison of pressure distribution for the bump in a channel in (a) selected position, (b) dimensionless form at the highest point of pressure

For wedge geometry, the grid independence test was carried out at the selected position, 0 to 0.2m. Six different grid sizes were tested to determine the effect on the pressure distribution, as shown in Figure 5(a). The pressure distribution at the highest point of pressure (0.11m) is shown in Figure 5(b). The graph is obtained by dividing all the pressure of different grid sizes by the pressure at Grid 3, 11352. At grid size 13112, which is Grid 2, the pressure distribution is nearly constant. Thus, a grid size of 14872, Grid 1 has been selected for wedge geometry.

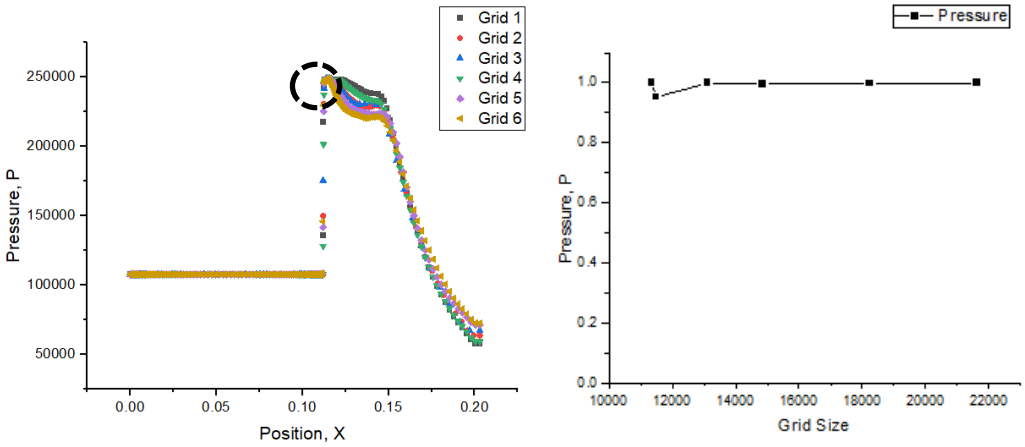

(a) (b)

Fig. 5. Comparison of pressure distribution for a wedge in (a) selected position, (b) dimensionless form at the highest point of pressure

Figure 6(a) shows pressure distribution for blunt-body from Grid 1 to Grid 6. The difference in pressure between the grid size at the highest point of pressure can be seen clearly in Figure 6(b). The pressure distribution fluctuates at grid size less than 5760 and increases afterwards. There are significant pressure changes as the optimum pressure has not been obtained yet. The grid size 5760, Grid 1 has been used to perform simulation for blunt-body geometry.

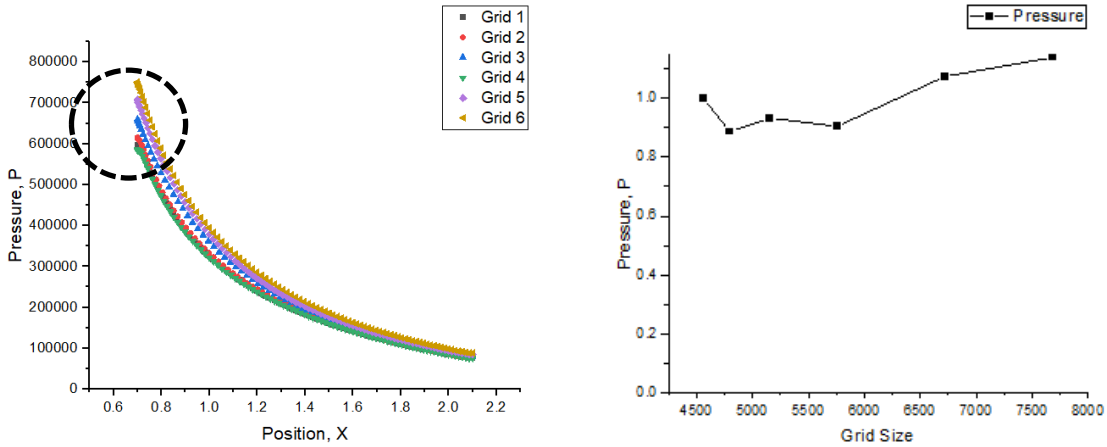

(a) (b)

Fig. 6. Comparison of pressure distribution for blunt-body in (a) selected position, (b) dimensionless form at the highest point of pressure

4. Results and Discussions

The results obtained by the codes' extension are compared to those obtained by Harada *et al.,* [21]. Figure 7(a) is the pressure contours for $M_\infty = 2.0$ (case 1) obtained by Harada is similar to the results shown in Figure 8. The modified Fourth-Order Runge-Kutta has been validated against the analytical solution for $M_\infty = 2.0$, as shown in Figure 7(b).

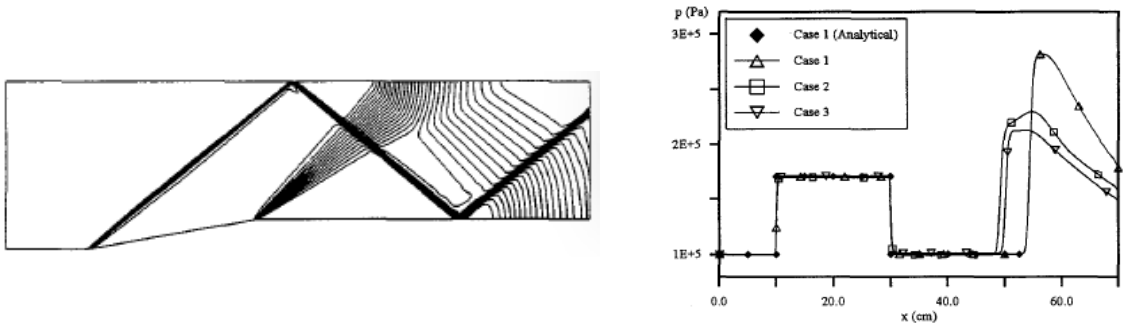

(a) (b)

Fig. 7. (a) Pressure contours for $M_\infty = 2.0$ by Harada, (b) Comparison of the pressure distributions on the lower surface for $M_\infty = 2.0$ by Harada

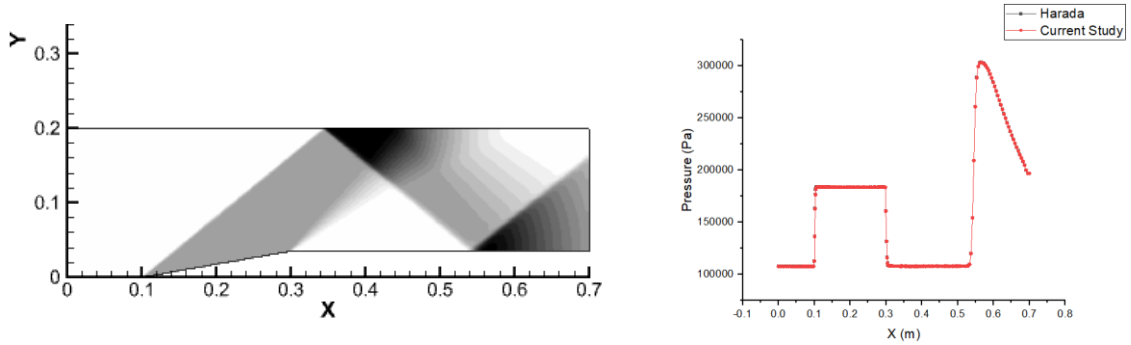

(a) (b)

Fig. 8. (a) Pressure contours for $M_\infty = 2.0$, (b) Comparison of the pressure distributions on the lower surface for $M_\infty = 2.0$

4.1 The Application of the Davis-Yee Upwind TVD Scheme

The first test case is an internal flow pass-through bump in a channel. The geometry of a bump channel can produce bow shocks, oblique shocks, and expansion waves, which are captured using the Davis-Yee upwind TVD scheme with different limiter functions. When the flow enters the channel and hits the bump, it will produce bow shocks and create reflection on the upper wall. In addition, it will generate wave interaction between the upper and lower oblique shock. The shocks do not result in a boundary-value separation near the entrance since they are not strong [22]. Figure 9 exhibits the same pattern but different values of density. Figure 9(a) shows that the strong oblique shock captured by the TVD scheme using limiter 1 has the highest density value compared to limiter 2 and limiter 3.

Figure 9(b) and Figure 9(c) exhibit almost the same density value compared to Figure 9(a). Therefore, based on the three limiters used, limiter 2 is the best as the density value is between the upper extremity and lower extreme, limiter 1 and limiter 3, respectively.

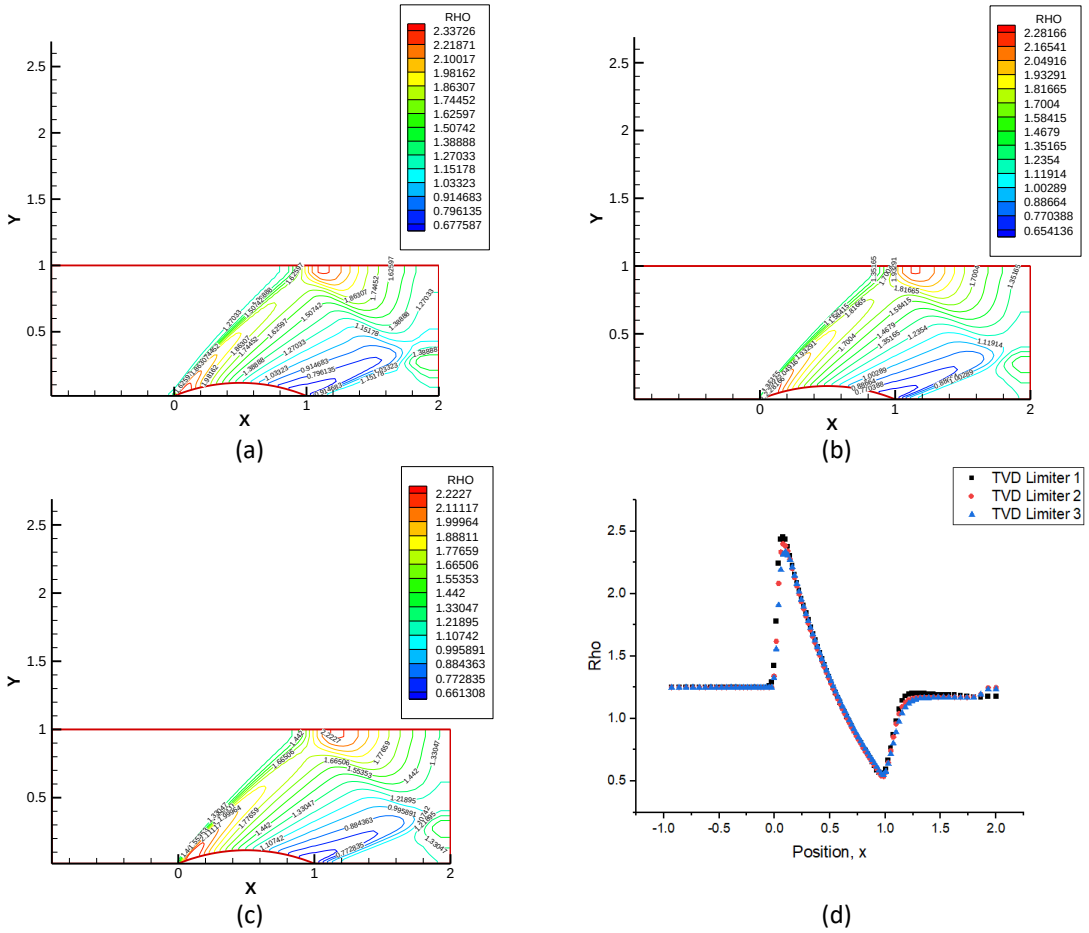

Fig. 9. Density contour of internal bump channel flow for $\boldsymbol{Ma = 2.0}$ using (a) limiter 1, (b) limiter 2, (c) limiter 3, (d) density distribution at selected area

Figure 10 displays the density contour for the internal flow pass-through wedge. As it can be seen, the oblique shock captured in Figure 10(a) is thinner and more compact than in Figure 10(b) and Figure 10(c). This is because oblique shocks refract at tangential discontinuities and intersect with other shock waves after reflecting from the walls [23]. The limiter functions used as the results depict a similar pattern, but the minimum and maximum density values are obtained by limiter 1. The highest and lowest density regions were identified behind the oblique shock wave and in the vortex region. A high-density region is generated as the oblique shock extends farther downstream [24].

All the limiter functions have almost the same density value. Still, limiter 2 had been chosen as the best to capture the shock wave rather than limiter 1 and limiter 3 as the density value is in the middle of the upper extreme and lower extreme.

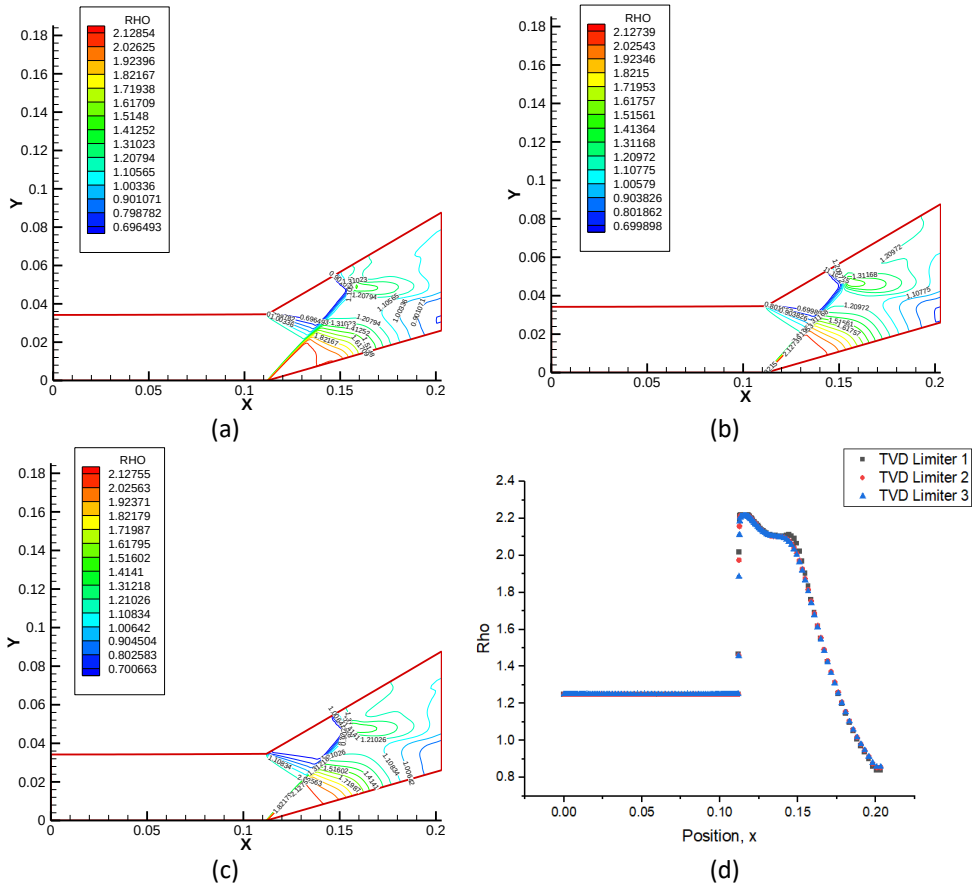

Fig. 10. Density contour of wedge flow for $\boldsymbol{Ma = 2.0}$ using (a) limiter 1, (b) limiter 2, (c) limiter 3, (d) density distribution at selected area

Figure 11 shows the density flow contour regarding the location of oblique shock waves with different limiter functions. When supersonic flow imparts a body with an angle of deviation, bow shocks can be observed on the blunt-body test case due to geometrically induced pressure, temperature, and density [25]. Limiter function 3 captured more compact bow shocks, as shown in Figure 11(c), compared to the bow shocks captured in Figure 11(a) and Figure 11(b). The highest density region was identified at the bottom of the blunt-body, and the highest density value was obtained using limiter 3.

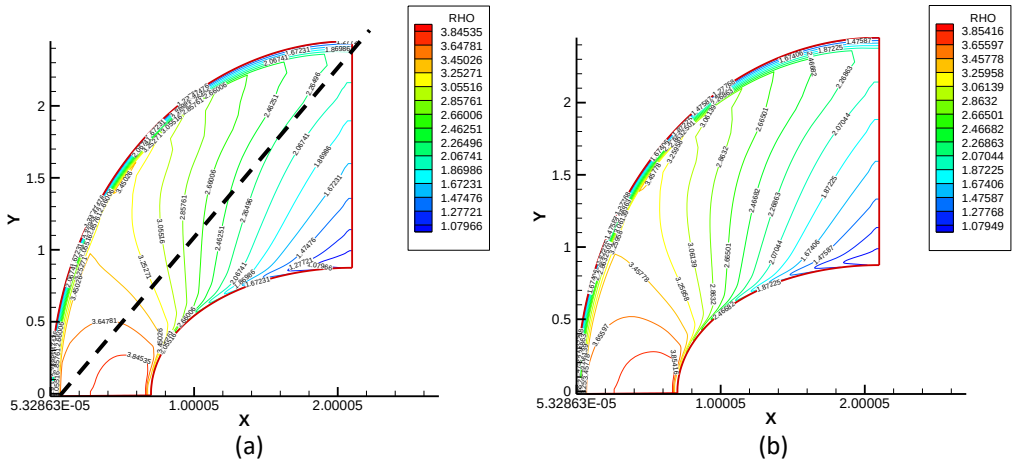

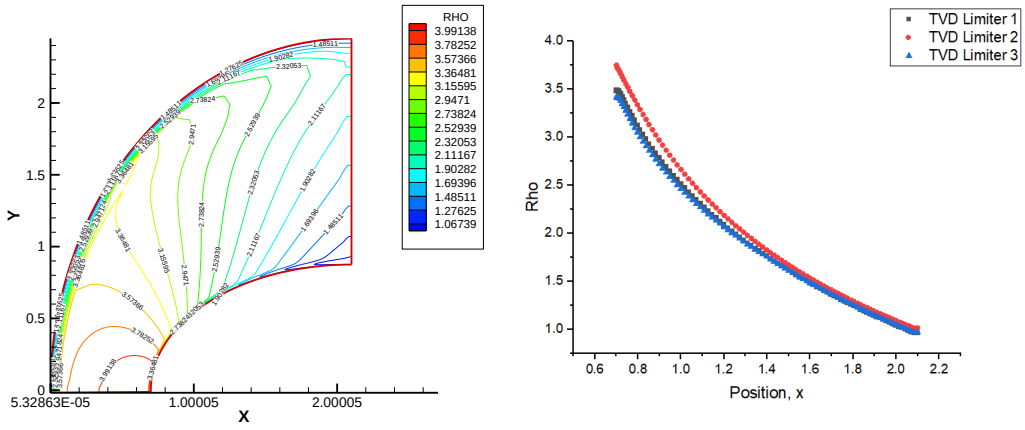

(c) (d)

Fig. 11. Density contour of external blunt-body flow for $\boldsymbol{Ma = 2.0}$ using (a) limiter 1, (b) limiter 2, (c) limiter 3, (d) density distribution at selected area

4.2 The Application of Harten-Yee Upwind TVD Scheme

Based on Figure 12, the density contour of external flow using limiter 1 shows different bow shocks and expansion waves locations compared to limiter 2 and limiter 3. The bow shocks captured using limiter 2 and limiter 3 can be seen nicely and easily understood compared to limiter 1 in Figure 12(a). Limiter 1 had made the Harten-Yee TVD scheme becomes a diffusive scheme, as shown in Figure 12(a), as minmod is more diffusive [26]. Figure 12(b) and Figure 12(c) depict a similar contour pattern to Figure 7, even though different schemes are used.

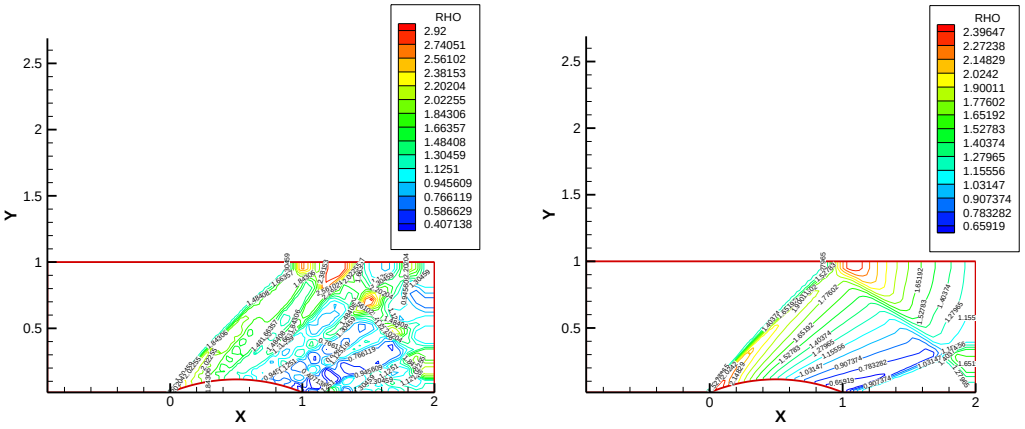

(a) (b)

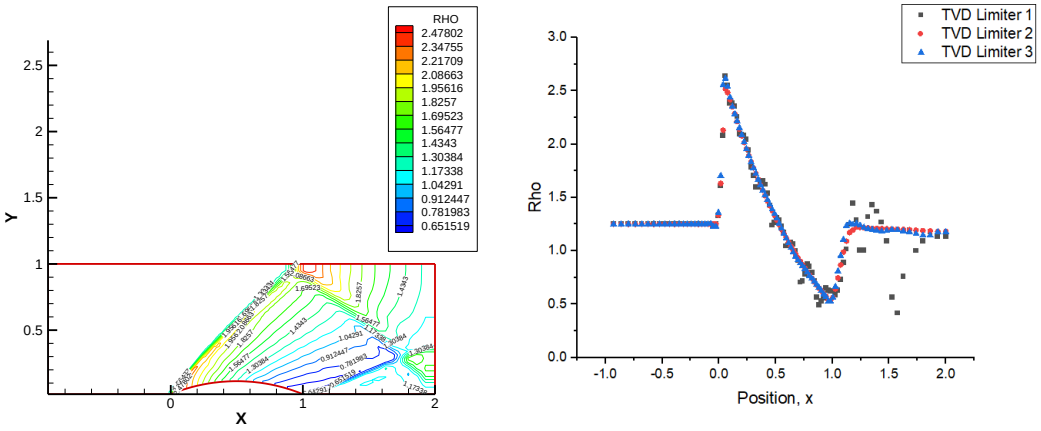

(c) (d)

Fig. 12. Density contour of internal bump channel flow for $\boldsymbol{Ma = 2.0}$ using (a) limiter 1, (b) limiter 2, (c) limiter 3, (d) density distribution at selected area

Based on the results obtained by the Harten-Yee Upwind TVD scheme and Davis-Yee Symmetric TVD scheme for the bump in a channel, as shown in Figure 9 and Figure 12, respectively, the Davis-Yee Symmetric TVD scheme is better at capturing shock wave, which is in this study in term of density. The density value for the Davis-Yee Upwind TVD scheme is not in the upper extreme or lower extreme compared to the Harten-Yee Upwind TVD scheme.

5. Conclusions

Based on the results, one can conclude that the Modified Fourth-Order Runge Kutta Scheme with TVD; Harten-Yee Upwind TVD scheme, or Davis-Yee Symmetric TVD scheme represents the algorithm that can be applied for analyzing supersonic internal flows as well as an external flow problem. There is no problem with the presence of various limiter functions. In the case of internal flow problems, high supersonics various flow features that may appear in the flow field, such as bow shock, oblique shock, shock wave reflection, interaction, and expansion wave, can be captured. While in the case of the external supersonic flow passing through the blunt-body, both Euler solvers are produced the same flow pattern, namely the presence of a bow shock wave. In the case we used in the study, we found that Davis-Yee limiter number 2 performs much better than other suggested Davis-Yee and Harten-Yee limiters. Therefore, for the same case on the extension of this study, the Davis-Yee Upwind TVD scheme is recommended. This Euler solver may be extended to the case of transonic flow passing through airfoils, making the solver more valuable since it will become an aerodynamics analysis tool.

Acknowledgement

The authors would like to express gratitude to the Ministry of Higher Education (MOHE) through Fundamental Research Grant Scheme (FRGS) (FRGS/1/2020/STG06/UTHM/02/3) & Universiti Tun Hussein Onn Malaysia for supporting this research.

References

[1] Sa, Luis FN, Carlos M. Okubo, and Emílio C. N. Silva. "Topology optimization of subsonic compressible flows." *Structural and Multidisciplinary Optimization* 64, no. 1 (2021): 1-22. https://doi.org/10.1007/s00158-021-02903-5

[2] Victoria Rolandi, Laura, Thierry Jardin, Jérôme Fontane, Jérémie Gressier, and Laurent Joly. "Stability of the low Reynolds number compressible flow past a NACA0012 airfoil." *AIAA Journal* 60, no. 2 (2022): 1052-1066. https://doi.org/10.2514/1.J060792
[3] Constantin, Peter, and Vlad Vicol. "Remarks on high Reynolds numbers hydrodynamics and the inviscid limit." *Journal of Nonlinear Science* 28, no. 2 (2018): 711-724. https://doi.org/10.1007/s00332-017-9424-z
[4] Ranocha, Hendrik, Lisandro Dalcin, Matteo Parsani, and David I. Ketcheson. "Optimized Runge-Kutta methods with automatic step size control for compressible computational fluid dynamics." *Communications on Applied Mathematics and Computation* (2021): 1-38. https://doi.org/10.1007/s42967-021-00159-w
[5] Sun, Zheng, and Chi-wang Shu. "Strong stability of explicit Runge--Kutta time discretizations." *SIAM Journal on Numerical Analysis* 57, no. 3 (2019): 1158-1182. https://doi.org/10.1137/18M122892X
[6] Bhatt, Ashish, and Brian E. Moore. "Structure-preserving Exponential Runge--Kutta Methods." *SIAM Journal on Scientific Computing* 39, no. 2 (2017): A593-A612. https://doi.org/10.1137/16M1071171
[7] Bai, Feng-peng, Zhong-hua Yang, and Wu-gang Zhou. "Study of total variation diminishing (TVD) slope limiters in dam-break flow simulation." *Water Science and Engineering* 11, no. 1 (2018): 68-74. https://doi.org/10.1016/j.wse.2017.09.004
[8] Lin, Lei, and Zhe Liu. "TVDal: Total variation diminishing scheme with alternating limiters to balance numerical compression and diffusion." *Ocean Modelling* 134 (2019): 42-50. https://doi.org/10.1016/j.ocemod.2019.01.002
[9] Saldía, J., S. Elaskar, and J. Tamagno. "Numerical simulations using tvd schemes of two-dimensional supersonic flow in chemical equilibrium." *International Journal of Computational Methods* 14, no. 2 (2017): 1750020. https://doi.org/10.1142/S0219876217500207
[10] de Goes Maciel, Edisson Savio, and Cláudia Regina de Andrade. "Comparison among unstructured TVD, ENO and UNO schemes in two-and three-dimensions." *Applied Mathematics and Computation* 321 (2018): 130-175. https://doi.org/10.1016/j.amc.2017.10.026
[11] Hou, Jingming, Qiuhua Liang, Zhanbin Li, Shifeng Wang, and Reinhard Hinkelmann. "Numerical error control for second-order explicit TVD scheme with limiters in advection simulation." *Computers & Mathematics with Applications* 70, no. 9 (2015): 2197-2209. https://doi.org/10.1016/j.camwa.2015.08.022
[12] Yadegari, Mitra, and M. H. Jahdi. "Capturing of Shock Wave of Supersonic Flow over the Bump Channel with TVD, ACM and Jameson Methods." *Iranian Journal of Mechanical Engineering Transactions of the ISME* 22, no. 1 (2021): 108-126.
[13] Farzi, Javad, and Fayyaz Khodadosti. "A total variation diminishing high resolution scheme for nonlinear conservation laws." *Computational Methods for Differential Equations* 6, no. 4 (2018): 456-470.
[14] Yee, Helen C. *On the implementation of a class of upwind schemes for system of hyperbolic conservation laws*. No. NAS 1.15: 86839. 1985.
[15] Harada, Shigeki, Justin Augustinus, Klaus Hoffmann, Ramesh Agarwal, Shigeki Harada, Justin Augustinus, Klaus Hoffmann, and Ramesh Agarwal. "Development of a modified Runge-Kutta scheme with TVD limiters for the ideal 1-D MHD equations." In *13th Computational Fluid Dynamics Conference*, p. 2090. 1997. https://doi.org/10.2514/6.1997-2090
[16] Reddy, Suryakumar, and Michael Papadakis. "TVD schemes and their relation to artificial dissipation." In *31st Aerospace Sciences Meeting*, p. 70. 1993. https://doi.org/10.2514/6.1993-70
[17] Hejranfar, Kazem, and Saman Rahmani. "Numerical simulation of shock-disturbances interaction in high-speed compressible inviscid flow over a blunt nose using weighted essentially non-oscillatory scheme." *Wave Motion* 88 (2019): 167-195. https://doi.org/10.1016/j.wavemoti.2019.03.014
[18] Hixon, R., S-H. Shih, T. Dong, and R. Mankbadi. "Evaluation of generalized curvilinear coordinate transformations applied to high-accuracy finite-difference schemes." In *36th AIAA Aerospace Sciences Meeting and Exhibit*, p. 370. 1998. https://doi.org/10.2514/6.1998-370
[19] Demirdžić, I., Ž. Lilek, and M. Perić. "A collocated finite volume method for predicting flows at all speeds." *International Journal for Numerical Methods in Fluids* 16, no. 12 (1993): 1029-1050. https://doi.org/10.1002/fld.1650161202
[20] Alfarawi, Suliman, Azeldin El-sawi, and Hossin Omar. "Exploring Discontinuous Meshing for CFD Modelling of Counter Flow Heat Exchanger." *Journal of Advanced Research in Numerical Heat Transfer* 5, no. 1 (2021): 26-34.
[21] Harada, Shigeki, Klaus Hoffmann, and Justin Augustinus. "Development of a modified Runge-Kutta scheme with TVD limiters for the ideal two-dimensional MHD equations." In *36th AIAA Aerospace Sciences Meeting and Exhibit*, p. 981. 1998. https://doi.org/10.2514/6.1998-981
[22] Kuzmin, Alexander. "Hysteresis of shock wave locations in divergent bent channels." *Computers & Fluids* 182 (2019): 52-59. https://doi.org/10.1016/j.compfluid.2019.02.016
[23] Bulat, Pavel, Anzhelika Melnikova, Vladimir Upyrev, and Konstantin Volkov. "Refraction of oblique shock wave on a tangential discontinuity." *Fluids* 6, no. 9 (2021): 301. https://doi.org/10.3390/fluids6090301

[24] Zhang, Yining, Pengfei Yang, Honghui Teng, Hoi Dick Ng, and Chihyung Wen. "Transition between different initiation structures of wedge-induced oblique detonations." *AIAA Journal* 56, no. 10 (2018): 4016-4023. https://doi.org/10.2514/1.J056831

[25] Landau, Lev Davidovich, and Evgenii Mikhailovich Lifshitz. *Fluid Mechanics: Landau and Lifshitz: Course of Theoretical Physics*, Volume 6. Vol. 6. Elsevier, 2013.

[26] Sanders, Brett F., and Scott F. Bradford. "Impact of limiters on accuracy of high-resolution flow and transport models." *Journal of Engineering Mechanics* 132, no. 1 (2006): 87-98. https://doi.org/10.1061/(ASCE)0733-9399(2006)132:1(87)